PAPER • OPEN ACCESS

Self-guided propagation of laser pulses reflected at high intensity from plasma mirrors

IOP Publishing New J. Phys. 27 (2025) 124302 https://doi.org/10.1088/1367-2630/ae2cbf

New Journal of Physics
The open access journal at the forefront of physics

Deutsche Physikalische Gesellschaft DPG
IOP Institute of Physics

Published in partnership with: Deutsche Physikalische Gesellschaft and the Institute of Physics

PAPER

Self-guided propagation of laser pulses reflected at high intensity from plasma mirrors

J-N Gruse[1], N C Lopes[1,2], R J Shalloo[1,3], J A Hills[1,*], A Alejo[4,5], T L Audet[4], M P Backhouse[1], N Bourgeois[6], E Gerstmayr[1], S P D Mangles[1], K Põder[3], P P Rajeev[6], S Rozario[1], G Sarri[4], M J V Streeter[1,4], J C Wood[1,3] and Z Najmudin[1]

[1] The John Adams Institute for Accelerator Science, The Blackett Laboratory, Imperial College London, London, United Kingdom
[2] GoLP, Instituto de Plasmas e Fusão Nuclear, Instituto Superior Técnico, Lisboa, Portugal
[3] Deutsches Elektronen-Synchrotron (DESY), Notkestrasse 85, Hamburg, Germany
[4] School of Mathematics and Physics, Queen's University, Belfast, United Kingdom
[5] Instituto Galego de Fisica de Altas Enerxias (IGFAE), Universidade de Santiago de Compostela, 15705 Santiago de Compostela, Spain
[6] Central Laser Facility, STFC Rutherford Appleton Laboratory, Didcot, United Kingdom
[*] Author to whom any correspondence should be addressed.

E-mail: jasmin.hills19@imperial.ac.uk and z.najmudin@imperial.ac.uk

Keywords: LWFA, staging LPA, electron acceleration, plasma mirror, wakefield properties

OPEN ACCESS

RECEIVED
14 August 2025

REVISED
28 November 2025

ACCEPTED FOR PUBLICATION
15 December 2025

PUBLISHED
29 December 2025

Abstract

The reflectivity and optical quality of laser pulses reflected off 125 μm Kapton™ tape was investigated for use as a repeatable plasma mirror. Reflectivities of around 70% were measured at $\approx 2 \times 10^{21}$ Wm^{-2} while maintaining the quality of the laser beam. The ability of the reflected pulse to drive a laser wakefield accelerator was investigated. Self-guided propagation of the reflected beam through a gas cell was observed and shown to depend on the plasma density. Particle-in-cell simulations showed that a wakefield would have been generated, driven solely by the energy within the central high intensity feature of the focal spot. The use of plasma mirrors at these elevated intensities would open up the possibilities of extremely compact configurations for laser wakefield accelerator stages.

1. Introduction

Laser plasma wakefield acceleration (LWFA) is a method of accelerating electrons to high energies using ultrashort, high-intensity laser pulses [1]. The high field strengths available in LWFA enable compact acceleration. Acceleration in a LWFA was first demonstrated experimentally using an externally injected electron beam [2]. Subsequent observation of self-injection and acceleration of electrons [3–5] has enabled the widespread adoption of these accelerators.

In the simplest configuration of LWFA, the maximum energy to which electrons can be accelerated is limited by diffraction of the laser beam, dephasing of accelerated electrons from the driving laser pulse, and depletion of the laser pulse energy [6]. Tailored plasma channels can be designed to overcome limitations due to diffraction [7–10], enabling the attainment of energies up to 10 GeV [11]. Spatiotemporal shaping of the driving pulse has been suggested as a way to accelerate electrons beyond the dephasing limit [12–14]. However, depletion of the laser energy is a more challenging limitation. The use of multiple acceleration stages driven by separate laser beams, commonly referred to as staging, is an intuitive method to replenish the depleted laser. Staging has been demonstrated for low electron energies ($\approx$ 100 MeV) at lower laser power [15]. In this work, we extend the staging concept to the higher power laser systems which would enable increased energy gain.

A compact setup, seen in figure 1(a), was used to test key aspects of staging. A laser beam can drive injection and acceleration of electrons in a gas cell, before being ejected by a Kapton tape. The tape acts as a plasma mirror, becoming highly reflective as plasma forms when the foot of the pulse reaches the tape. This discards any remaining laser energy exiting the gas cell. A second laser beam can then be reflected onto the optical axis by an additional tape-based plasma mirror. Plasma mirrors formed

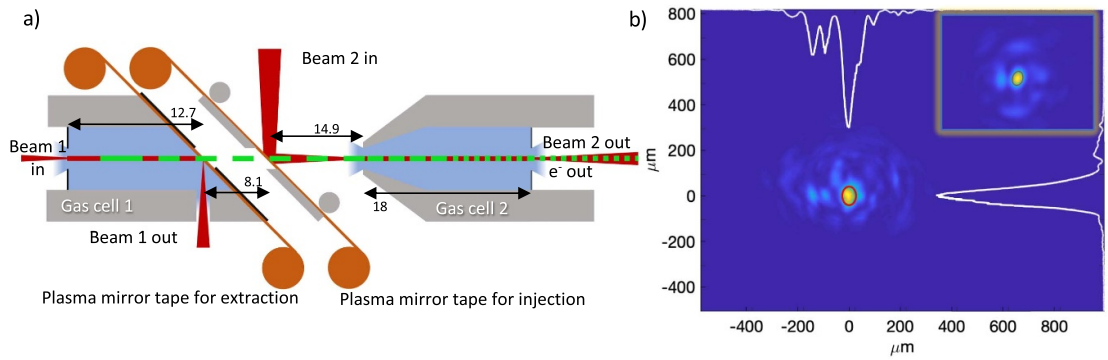

Figure 1. (a) Schematic of the two stage accelerator (lengths in mm). Laser beam 1 enters from the left, driving a wakefield in gas cell 1, before being dumped by a tape-based plasma mirror. Beam 2 is then reflected by a separate plasma mirror into gas cell 2. Accelerated electrons from cell 1 would travel through both sets of tape into cell 2. (b) The beam profile at focus is shown after reflection from the tape with the red ellipse indicating the FWHM; line-outs along the long (major) and short (minor) axis of the ellipse are given in white; the inset depicts the equivalent far-field beam profile of the incident beam without the plasma mirror, as measured with a microscope objective at low power.

from anti-reflection (AR) coated mirrors have been extensively studied. The AR mirror allows the low intensity foot of the pulse to be mostly transmitted whilst reflecting the high intensity peak of the pulse, improving the contrast ratio of high intensity laser systems [16–29]. However, plasma mirrors can also be used to redirect beams near focus. This can be useful for driving laser wakefield accelerator stages, which require large focal spots and so employ long focal length focusing optics. Without a plasma mirror, this would necessitate long distances between stages, reducing their mean acceleration. The plasma mirror allows a high intensity laser pulse to be injected orthogonal to the acceleration axis, as in figure 1(a), helping to make the system more compact [30, 31].

In our setup, the reflected beam was directed into a second gas cell, located less than 15 mm away, where this beam can drive a wakefield. If properly timed, an electron beam generated in the first cell (injector) can pass through the tapes and be injected into the accelerating phase of the wakefield in the second cell (accelerator), as demonstrated in [15]. Tape-based plasma mirrors do not yet offer contrast enhancement, but they can be operated at higher repetition rate [32], which is highly desirable for driving wakefield accelerators. The use of tape-based plasma mirror systems to drive laser driven plasma stages was established in [15]. In earlier work, they showed that the reflectivity of tape-based plasma mirrors increased up to on-tape intensities as high as $3 \times 10^{21}\,\mathrm{Wm}^{-2}$ [30, 31]. This is still below the intensities at which the interaction becomes strongly relativistic ($>10^{22}\,\mathrm{Wm}^{-2}$), at which point absorption naturally increases due to vacuum heating mechanisms [33, 34]. Tape-based mirrors were found to have reflectivities comparable to those based on dielectric mirrors at these elevated intensities [19, 26]. These measurements were limited to laser energies of ∼650 mJ, which restricted the energy gain of the corresponding wakefield stage to a few hundred MeV [15].

Here, we extend the measurements of the reflectivity of tape-based plasma mirrors to laser pulses with energies >1 J, as would be necessary for multi-GeV acceleration [11, 35]. As well as the reflectivity, we characterise the quality of the reflected beam, since this is critical to enabling wakefield generation in the accelerator stage. Even with a relatively poor laser wavefront onto the plasma mirror, we find high reflectivities (in excess of 70%) can be achieved at high laser powers. The guiding properties of the reflected laser beam were investigated by focusing it into a gas cell. Measurements of laser energy and beam profile were taken after transmission through the gas cell. Evidence for guided propagation was observed, showing that the plasma mirror reflected beam is suitable for driving a LWFA. The measurements were compared to the output of simulations performed using the particle-in-cell (PIC) code EPOCH in 2D [36]. These simulations improve our understanding of the propagation of the laser pulse and the wakefield that it forms in the second gas cell.

2. Experimental set-up for high intensity plasma mirror

The experiment was performed using the Gemini laser system at the Rutherford-Appleton Laboratory. Gemini is a high power Ti:sapphire CPA system featuring two laser beams, each of which can deliver up to ∼10 J on target in pulse lengths $\tau_{\mathrm{FWHM}} \leqslant 42$ fs [37] at a central wavelength $\lambda_0 \approx 800$ nm. As this work solely explores the second (accelerator) stage of the set-up, the experimental description is limited to the

reflection and guiding of the accelerator stage laser beam. However, the injector stage laser beam was used for diagnostic calibration.

A 7500 mm focal length dielectric spherical mirror was used to focus the laser pulse from an initial beam diameter of 100 mm (i.e. $f/75$ focussing). An adaptive optic (deformable mirror) was used to obtain a near-diffraction limited spot size with highest encircled energy at focus when focussing without the tape. As depicted in figure 1(a), a tape drive with Kapton tape was inserted to reflect the laser beam 14.9 mm before it reached its focus. After each shot, the drive was advanced to a fresh piece of the tape. The tape was stopped and tensioned over a metal guide between shots. Uncertainties along the focusing axis should be dominated by the variations in the thickness of the tape (which is less than 0.07 μm [38]) and its subsequent expansion. The tape was found to increase the uncertainty in pointing to 4.0 μm off the tape as compared to the intrinsic laser pointing stability of 1.9 μm. Hence, the tape introduces an extra $\sim$0.5 mrad of pointing error, which is comparable to previous measurements [30]. A *s*-polarised pulse was used to avoid Brunel absorption [33, 39], which decreases the reflectivity of the plasma mirror [31]. For the highest laser energy used here (7.3 J), the intensity on the tape would be $3.6 \times 10^{21}\,\mathrm{Wm}^{-2}$.

The laser beam was collimated after reflection from the tape using a 3175 mm focal length Au-coated spherical mirror. The beam was reflected off two glass wedges before leaving the vacuum chamber, thus reducing the *B*-integral in the exit window to $B \approx 0.53$. The collimated beam was refocused by another (on-axis) Au-coated spherical mirror with a focal length of 2000 mm. The focusing beam was split by a glass wedge to allow simultaneous measurement of the far-field focal beam quality and the transmitted energy. For the far-field measurement, the reflection off the wedge was imaged onto an *Andor Neo* 2160×2560 *sCMOS* camera.

The far-field was spatially calibrated by using a grating with a spacing of $d = 7$ mm placed in the collimated beam before the final focussing optic in the imaging system. The resulting diffraction pattern has maxima at $\sin\theta = m\lambda/d$, with m being the order of a maximum and where θ is the angle between the optical axis and the camera. The deflection of the mth order on the camera is then given by $x_m = mf\tan\theta$, where the focal length of the optic used to image the beam was f. The far-field of the beam before reflection from the plasma mirror was measured by removing the plasma mirror and imaging the laser with an objective at low laser power. An example of this 'pre-reflection' far-field is depicted in the inset of figure 1(b). The average spot size was 64 ± 17 μm in this experiment, which is comparable to the diffraction limit. Before reflection, the energy within the full-width half-maximum (FWHM) was $(19.2 \pm 1.8)\%$ compared to 50% expected in the FWHM for an ideal Gaussian beam. The reduction in encircled energy (compared to the ideal case) is thus the main factor in determining the Strehl ratio (ratio of measured peak intensity to theoretical peak intensity) of the beam.

The energy passing through the final wedge was passed onto a *Gentec QE8SP-B-BL-D0* energy meter, which served as a transmitted laser energy diagnostic. This was calibrated using the laser beam from the injector stage with gas cells and plasma mirrors removed. This was done as the reflection of the second laser beam onto the optical axis would have produced a plasma even in its lowest power mode, making the calibration of the downstream diagnostics unpredictable. The two laser beams were orthogonally polarised. Therefore, a waveplate was introduced to make the calibration beam *s*-polarised, the same as the pulse reflected off the plasma mirror. The energy calibration was done in two steps; first, a second *Gentec QE25SP-S-MB* was placed in the vacuum chamber and the energy of the calibration beam was measured close to focus at low power. This energy meter was then removed, and the pulse energy outside the chamber, after passing through the forward line optics, was measured. This allowed the transmission factor of the collection optics to be determined.

3. Reflectivity and beam quality of high intensity plasma mirror

The reflectivity of the plasma mirror, for total incident energy up to ≈ 8 J, can be seen in figure 2(a) in red. The measured reflectivity peaks at $(73.7 \pm 8.9)\%$ at 4 J, corresponding to an intensity of $2 \times 10^{21}\,\mathrm{Wm}^{-2}$, which is in line with previous measurements [30, 31]. The reflectivity fell at higher energies. Such a drop-off in reflectivity for plasma mirrors at higher incident intensities is usually attributed to the adverse effect of pre-plasma formation [26, 31, 40]. In our case, the slower than typical fall-off in plasma reflectivity is likely to be due to the poor spatial profile of the laser profile, both in phase and intensity, due to laser damage on the turning mirrors. As a result, the range of intensities witnessed locally on the plasma mirror had a greater variation than the mean quoted here, broadening the range of energies over which the drop-off behaviour is witnessed.

However, it is the energy in the central high intensity spot in the far-field which is most important for driving a wakefield. Figure 1(b) shows an example far-field image of the reflected beam from the plasma mirror. The beam has a total reflectivity of 72% at an input energy of 5.5 J for a corresponding

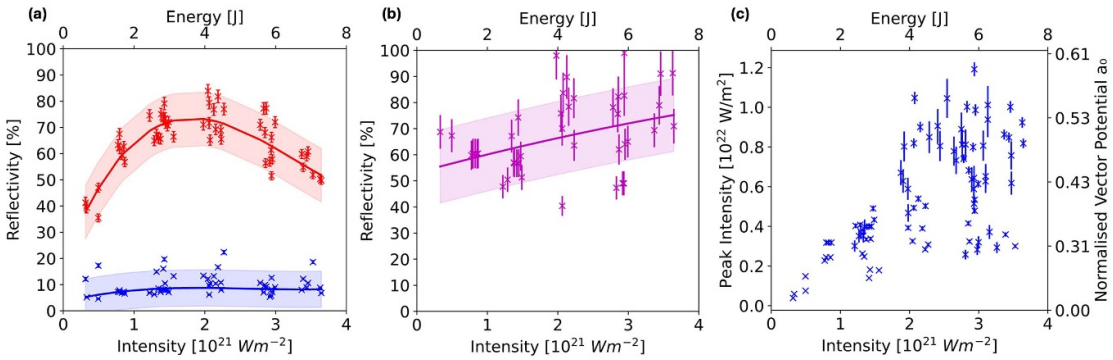

Figure 2. Reflectivity measurements as a function of intensity (energy) on the plasma mirror: (a) total reflectivity (red) and fraction of total energy reflected within FWHM (blue). (b) Energy in the far-field FWHM of the reflected beam as compared to that for the beam before reflection. Lines are fitted with a 3rd order splines. (c) The intensity and a_0 of the reflected laser beam at best focus (i.e. at the gas cell entrance).

on-mirror intensity of $2.8 \times 10^{21}\,\mathrm{Wm}^{-2}$, resulting in $>4\,\mathrm{J}$. The FWHM of the encircling ellipsoid is depicted in red. A significant part of the energy lies outside the FWHM. Though the reflected beam only contains 12.2% of the total incident energy within the encircled FWHM, figure 2(b) shows that the ratio between the energy within the FWHM of the far-fields in the reflected and incident beams varies less than the total reflectivity. This ratio is on-average $(69 \pm 17)\%$, comparable to the peak total reflectivity. Since our tape is within a Rayleigh range ($z_R = 16\,\mathrm{mm}$) of best focus, it appears that the reflectivity of the high intensity part of the beam profile remains high even though the total reflectivity is falling with increasing on-tape intensity. This 'spatial filtering' effect has been reported before [19], and is usually attributed to the decreasing reflectivity of high spatial frequency components in the incoming beam profile. Spatial filtering can be controlled by changing the distance to focus, impacting the amount of the beam profile above the ionisation threshold on the plasma mirror. With increasing intensity, this would tend to increase reflectivity, but what we see is a decrease in reflectivity. We attribute this to the less focussed parts of the beam having a lower threshold at which reflectivity drops due, as noted above, to intensity and phase variations.

The measurements suggest that higher total energy reflectivity could be achieved for better initial beam profiles, i.e. if more energy had been in the original high intensity spot. As a consequence of the high reflectivity of the highest intensity spot, despite the decreasing over-all reflectivity, the intensity at best focus was still found to increase with increasing on-tape intensity. Accounting for the energy in the FWHM and the focussing optic used in the experiment, the normalised vector potential incident on the gas cell peaks around $a_0 = 0.6$, as seen in figure 2(c). This would result in wakefield production in the linear regime [6].

4. Guiding of a plasma-mirror reflected laser pulse

The suitability of the reflected laser pulse for driving wakefield was tested by determining its ability for self-guided propagation. The beam was passed, after reflection from the plasma mirror, into a helium gas cell with a fixed length of 18 mm. The gas cell length is comparable to the Rayleigh range $z_R \approx \pi {w_0}^2/\lambda \approx 16\,\mathrm{mm}$ for the input spot size of $w_0 = 63.7\,\mu\mathrm{m}$. Without any self-focusing effect, one would expect an increase in the spot size to $w \approx \sqrt{2} w_0$ over the length of the gas cell. For these shots, the input energy was $E_\mathrm{L} = (6.6 \pm 0.2)\,\mathrm{J}$ with $\approx 70\%$ reflected from the plasma mirror, corresponding to a laser power of $P_\mathrm{L} \approx 150\,\mathrm{TW}$ at the gas cell entrance. Lasers with power exceeding the critical power for relativistic self-focussing ($P > P_\mathrm{cr} \approx 17(n_\mathrm{cr}/n_e)\,\mathrm{GW}$) can be self-guided [41–43], with the help of refraction in the cavity of the wakefield that they generate [44, 45]. Here $n_\mathrm{cr} \simeq 1.7 \times 10^{27}\,\mathrm{m}^{-3}$, so self-focusing should be operative for densities greater than $n_\mathrm{e} \approx 2 \times 10^{23}\,\mathrm{m}^{-3}$. At these intensities ($a_0 < 1$), the laser will be guided with a matched spot size comparable to the wavelength of the relativistic plasma wave $\lambda_\mathrm{p} = \sqrt{n_\mathrm{cr}/n_\mathrm{e}} \cdot \lambda_0$ [45]. These simple considerations are usually only valid for idealised beams. It might be argued that the condition for self-focussing should only account for the energy within the high intensity spot, increasing the threshold density for self-focusing. Hence, the guiding properties of this beam had to be determined experimentally.

The gas cell density was varied and the transmitted spot size at the exit of the gas cell was measured. The right pane of figure 3(a) gives examples of the transmitted spot at two different densities. The

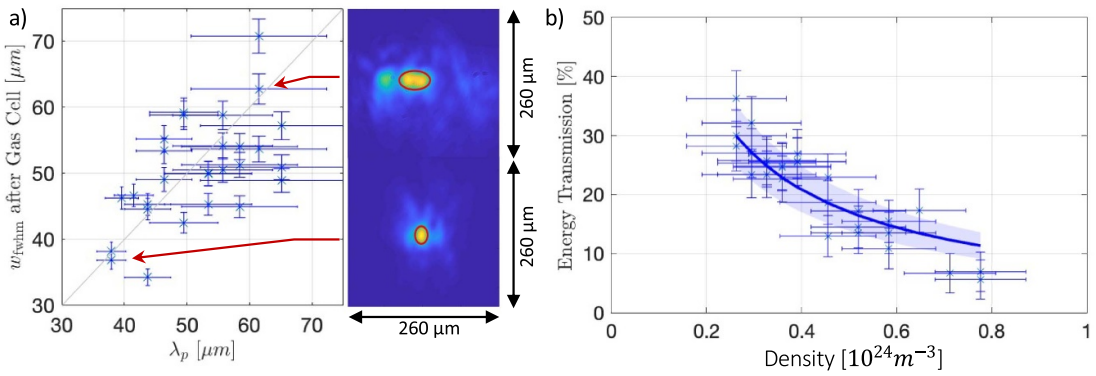

Figure 3. a) Measured focal spot size w_{fwhm} after the gas cell depending on the plasma wave wavelength λ_{p}. Example laser spots on the right for the lowest (upper : $(0.29 \pm 0.10) \times 10^{24}\,\mathrm{m}^{-3}$) and highest (lower : $(0.78 \times 0.10) \times 10^{24}\,\mathrm{m}^{-3}$) density investigated. (b) The energy transmitted through the gas cell relative to the energy incident on the gas cell against plasma density for input energy (6.6 ± 0.2) J. The blue line follows the fit $(1 - \exp(-2g\lambda_{\mathrm{p}}^2/\overline{w}^2))$ with $\overline{w} = 55.9\,\mu$m being an average spot size and g being a fitting parameter with best-fit of $g = 0.13^{+0.03}_{-0.03}$.

upper one is for a density of $(0.29 \pm 0.10) \times 10^{24}\,\mathrm{m}^{-3}$ for which the average transmitted spot size was $(62.8 \pm 2.3)\,\mu$m. The lower one is at a higher density of $(0.78 \pm 0.10) \times 10^{24}\,\mathrm{m}^{-3}$ for which the spot size has decreased to $(38.2 \pm 1.4)\,\mu$m. Figure 3(a) also plots the spot size at the exit of the cell against λ_{p} as it varies with density. Despite the large spread, there is an observable trend for the guided spot size to follow the plasma wave wavelength $w_{\mathrm{fwhm}} \approx \lambda_{\mathrm{p}}$. This provides evidence of self-guided propagation of the plasma mirror reflected pulse.

The backing pressure of the gas cell was correlated with the internal density using interferometry early in the experiment. However, laser damage to the to the gas cell entrance and exit apertures may have introduced a systematic error, producing a lower cell density for a given backing pressure. This is reflected in the large uncertainty in the measured densities in figure 3(a). The energy transmitted through the gas cell varied with plasma density. Figure 3(b) shows that the measured transmitted energy decreases for increasing plasma density at a constant incident energy on the plasma mirror of (6.6 ± 0.2) J. At the lowest density investigated, only $\approx 30\%$ of the total energy incident on the plasma mirror is transmitted through the cell, which is reduced to $< 10\%$ at the highest density investigated.

This energy loss cannot be attributed to ionisation. The energy required to fully ionise a column of helium of radius $r \approx w_0$ is $\mathcal{E}_{\mathrm{ion}} \approx \frac{1}{2} n_{\mathrm{e}} \pi w_0^2 L \sum_i \epsilon_i$, where $\sum_i \epsilon_i$ is the sum of ionisation energies and $\frac{1}{2} n_{\mathrm{e}}$ is the density of helium atoms. For a spot of $w_0 = 60\,\mu$m at $n_{\mathrm{e}} = 1 \times 10^{24}\,\mathrm{m}^{-3}$ only $\mathcal{E}_{\mathrm{ion}} = 1.2$ mJ [46] is required, which is small compared to the observed energy loss. Another source of energy loss is the creation of a wakefield. The energy depletion length for $a_0 < 1$ is given by $L_{\mathrm{pd}} \approx (1/a_0^2)\,(n_{\mathrm{cr}}/n_{\mathrm{e}})\,c\tau_{\mathrm{FWHM}}$ for $c\tau_{\mathrm{FWHM}} < \lambda_{\mathrm{p}}/2$ [45]. Considering the highest density and a_0 investigated here, $n_{\mathrm{e}} = 0.78 \times 10^{24}\,\mathrm{m}^{-3}$ and $a_0 = 0.6$, the depletion length yields $L_{pd} = 78$ mm. Over the 18 mm of our gas cell, we would thus not have expected more than 20% loss in transmitted energy. However, if the same laser energy was focused into a spot of nearly half its initial radius, as suggested by figure 3(a), this would lead to a doubling in a_0, and a factor of four reduction in depletion length. This would then be comparable to our interaction length, accounting for the greater energy loss at higher density. This suggests that self-focusing plays a role in the propagation properties of the reflected pulses. To further understand this behaviour, a series of PIC simulations were performed.

5. Simulations of wakefield generation and expected energy gain

The PIC code EPOCH was employed in 2D to evaluate the guiding properties of the reflected beam. Though 2D simulations do not give a full description of the guiding results presented above, they can give an indication of the focussing properties of the imperfect beams reflected from the plasma mirror. Hence, two separate sets of simulations were performed based on the example spot in figure 1(b), which has an elliptical shape of $(71.9 \pm 3.7) \times (43.5 \pm 2.3)\,\mu$m. The simulated beam profiles were generated to approximate the summed profiles along the semi-major and minor axes, as shown in white in figure 1(b). The semi-major axis (to the right in figure 1(b) was well represented by a single-mode Gaussian. For the semi-minor axis, a good representation of the beam's intensity profile (shown to the top) can be reproduced by using 7 displaced Gaussian modes. This simplified model of the beam does

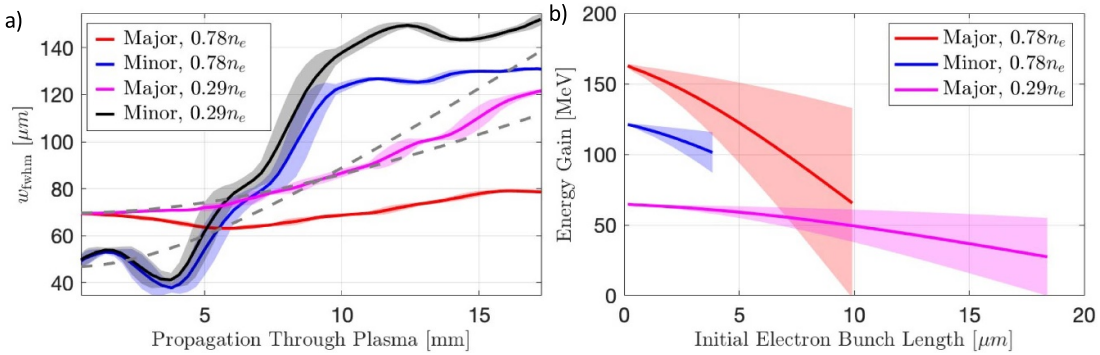

Figure 4. (a) Evolution of spot size for beam profiles modelled on the semi-major (Major) and semi-minor (Minor) axes at $0.78 \times 10^{24}\,\mathrm{m}^{-3}$ ($0.78n_e$: red, blue) and $0.29 \times 10^{24}\,\mathrm{m}^{-3}$ ($0.29n_e$: magenta, black). Dashed lines indicate the Gaussian spot size evolution in vacuum for both initial beam sizes. (b) Mean energy and FWHM energy spread for an initially top-hat temporal profile electron beam injected into the wakefield depending on initial bunch length. The result for semi-minor axis profile at $0.29 \times 10^{24}\,\mathrm{m}^{-3}$ is not included, as the focusing field of the wakefield is unstable.

not account for wavefront errors that degrade beam quality. Simulations were performed at the lowest and highest densities explored experimentally, $0.29 \times 10^{24}\,\mathrm{m}^{-3}$ and $0.78 \times 10^{24}\,\mathrm{m}^{-3}$ respectively, at a laser intensity of $0.89 \times 10^{22}\,\mathrm{Wm}^{-2}$ ($a_0 = 0.65$). The chosen densities correspond to $\lambda_\mathrm{p} = 62\,\mu$m and $37.8\,\mu$m. The guiding properties of these simulations are shown in figure 4.

Given a laser pulse of $E_\mathrm{L} = 6.6\,\mathrm{J}$ ($P \approx 150\,\mathrm{TW}$) entering the gas cell, the ratio of the laser power to the critical power for relativistic self-focusing, P/P_cr, falls between 1.5–4.0 for 2.9×10^{23}–$7.8 \times 10^{23}\,\mathrm{m}^{-3}$. The actual beams considered here contain as little as 38% of this total input energy, resulting in a lower ratio to the critical power, $P/P_\mathrm{cr} \approx 0.3$–$0.8$. These values suggest that due to poor beam quality, the guiding effect should be weak. The evolution of the spot size in the simulations is shown in figure 4(a). Considering only the major axis, the results indicate a lack of available energy for self-focusing. At lower density ($0.29n_c$, magenta line), the spot size evolution resembles the expected expansion in a vacuum. At higher density ($0.78n_c$, red line), the spot is found to self-focus over 5 mm, down to below $\approx 60\,\mu$m, and then remain relatively unchanged.

The simulations of the semi-minor axis (multiple Gaussians) are more interesting. There is a strong self-focusing effect for both densities ($0.29n_c$, black line and $0.78n_c$, blue line). In both cases, the pulse focuses down to below λ_p before expanding at faster than the vacuum rate of diffraction. The latter (semi-minor axis) simulations indicate that the higher-order modes contribute to the guiding of the laser pulse. This increases the pulse intensity, amplifying the self-focusing effect. However, the pulse focuses to below the matched spot size causing stronger subsequent defocusing. This behaviour is accentuated at higher densities, explaining the greater energy loss with increasing density seen in figure 3(b). Hence, though these simulations do not give a full 3D description of the interactions, they do demonstrate that the energy outside the high intensity focal spot helps to increase the self-focusing effect. However, paradoxically, this does not lead to better guided propagation.

Though stronger focusing leads to large wakefield generation, the restricted propagation also has an effect on the acceleration process. In the simulations, wakefields were generated as high as $10\,\mathrm{GV\,m}^{-1}$ at the higher density, which is inline with the predictions of the maximum expected electric field strength in the linear regime $E_\mathrm{wf} \approx {a_0}^2 E_0$, where $E_0 = m_\mathrm{e} c \omega_\mathrm{p}/e$ is the cold wavebreaking limit. The wakefield strength is similar for the initial profiles considered across both axes. However, the electric field drops more rapidly for simulations along the minor axis. At lower density, the difference between the two axes is much less pronounced, with both profiles producing initial fields of order $5\,\mathrm{GV\,m}^{-1}$, which slowly decrease in amplitude as the laser propagates through the cell.

The on-axis electric field of the wakefield generated in the simulations was used to estimate the energy gain that could have been achieved if an electron beam from the first gas cell had been successfully synchronised to the accelerator stage. An electron beam with flat-top temporal profile of varying pulse length was initiated behind the laser pulse in different phases of the wakefields and propagated with the speed of light. The energy gain was determined over the focusing phase of the wakefield. The *mean* energy gain (solid lines) over a variety of initial electron bunch lengths for the different simulations are shown in figure 4(b), with the bunch energy spread shown as the (shaded) bounds. Note this is the FWHM *not* total energy spread. The simulation based on the semi-minor axes of the laser profile at lower density is not shown, because the focusing field of the wakefield was unstable, with a low

accelerating field unsuitable for electron acceleration. Energy gain exceeds ≈150 MeV for the simulation along the semi-major axis. Despite the lower intensity and maximum electric field generated by the semi-major axis, the gain is higher due to the relatively constant spot size and more controlled acceleration experienced by the electrons. For a laser pulse profile averaged between the major and minor axis, a resulting energy gain of between ≈84 MeV–120 MeV would have been produced based on figure 4(b) at the higher density.

6. Conclusions and note on future optimisation of beam quality

Though not directly measured, the simulations based on the major-axis laser beam profile do support the generation of a wakefield which could have increased the energy of a relativistic electron beam by more than 150 MeV at these laser intensities. However, this is complicated by a non-ideal beam profile. Simulations based on the laser beam profile deviating more from an optimal Gaussian shape showed less laser guiding, with the acceleration of electrons inside the wakefield strongly depending on the density. For injection with a GeV level electron beam, the energy gain would have been only a fraction of the initial energy, thus making it challenging to observe. Nevertheless, it has been demonstrated that plasma mirrors can be used with high reflectivity at high intensity. Furthermore, the beam quality reflecting off the plasma mirror set-up used here did not degrade significantly at operating intensities on the plasma mirror of $(3.3 \pm 0.1) \times 10^{21}\,\mathrm{Wm}^{-2}$, as seen in figure 2(b). This greatly increases the options for compact staging configurations at high laser energy.

The primary factors limiting the reflected beam quality seem to be preplasma formation beyond a certain intensity threshold, and in this case, the poor quality of the input beam. Both of these factors can be improved in future experiments, in particular by improvements in temporal contrast of the laser pulse [20]. Using a maximum total energy of 15 J, with up to 33% of this energy contained within the far-field FWHM (comparable to previous measurements [47]), and assuming reflection from a plasma mirror with 70% reflectivity, the resulting peak intensity would be $5.7 \times 10^{22}\,\mathrm{Wm}^{-2}$, corresponding to $a_0 = 1.6$. Simulations performed with such characteristics indicate a wakefield with maximal accelerating field, $65\,\mathrm{GV\,m}^{-1}$ leading to a possible energy gain of 920 MeV. Further optimisations, such as using a smaller focus spot size and a corresponding higher density to match the pulse length, would increase the theoretical energy gain. Such optimisation would enable one to consider use of staged laser wakefield accelerators to overcome the depletion and dephasing limits. As a result, staged laser wakefield acceleration may thus make high-energy physics applications, such as the search for dark photons [48] and linear particle colliders [49], available on a more compact scale.

Data availability statement

All data that support the findings of this study are included within the article (and any supplementary files).

Acknowledgments

We acknowledge funding from STFC for the support of the John Adams Institute of Accelerator Science by Grants ST/J002062/1, ST/P000835/1, ST/V001639/1 and UKRI1888. EPOCH was developed under UK Engineering and Physics Sciences Research Council Grants EP/G054940/1, EP/G055165/1 and EP/G056803/1.

ORCID iDs

J-N Gruse 0000-0002-4099-8341
N C Lopes 0000-0001-8355-4727
R J Shalloo 0000-0002-9568-3814
J A Hills 0009-0003-5786-4846
A Alejo 0000-0002-6536-3828
M P Backhouse 0009-0005-5594-9154
N Bourgeois 0000-0003-4919-3977
E Gerstmayr 0000-0003-1164-8593
S P D Mangles 0000-0003-2443-4201
K Põder 0000-0002-0329-3510
P P Rajeev 0000-0002-7375-0000

S Rozario 0000-0001-7440-7821
G Sarri 0000-0003-1800-343X
M J V Streeter 0000-0001-9086-9831
J C Wood 0000-0003-4413-7044
Z Najmudin 0000-0001-6323-4005

References

[1] Tajima T and Dawson J M 1979 *Phys. Rev. Lett.* **43** 267–70
[2] Amiranoff F *et al* 1995 *Phys. Rev. Lett.* **74** 5220–3
[3] Mangles S P D *et al* 2004 *Nature* **431** 535–8
[4] Geddes C G, Toth C, Tilborg J V, Esarey E, Schroeder C B, Bruhwiler D, Nieter C, Cary J and Leemans W P 2004 *Nature* **431** 538–41
[5] Faure J, Glinec Y, Pukhov A, Klselev S, Gordienko S, Lefebvre E, Rousseau J P, Burgy F and Malka V 2004 *Nature* **431** 541–4
[6] Esarey E, Schroeder C B and Leemans W P 2009 *Rev. Mod. Phys.* **81** 1229–85
[7] Durfee C G and Milchberg H M 1993 *Phys. Rev. Lett.* **71** 2409–12
[8] Kaganovich D, Sasorov P, Cohen C and Zigler A 1999 *Appl. Phys. Lett.* **75** 772–4
[9] Spence D J, Butler A and Hooker S M 2003 *J. Opt. Soc. Am. B* **20** 138
[10] Kim M S, Jang D G, Lee T H, Nam I H, Lee I W and Suk H 2013 *Appl. Phys. Lett.* **102** 100–103
[11] Picksley A *et al* 2024 *Phys. Rev. Lett.* **133** 255001
[12] Sainte-Marie A, Gobert O and Quéré F 2017 *Optica* **4** 1298
[13] Palastro J, Shaw J, Franke P, Ramsey D, Simpson T and Froula D 2020 *Phys. Rev. Lett.* **124** 134802
[14] Caizergues C, Smartsev S, Malka V and Thaury C 2020 *Nat. Photon.* **14** 475–9
[15] Steinke S *et al* 2016 *Nature* **530** 190–3
[16] Kapteyn H C, Szoke A, Falcone R W and Murnane M M 1991 *Opt. Lett.* **16** 490
[17] Ziener C, Foster P S, Divall E J, Hooker C J, Hutchinson M H, Langley A J and Neely D 2003 *J. Appl. Phys.* **93** 768–70
[18] Doumy G, Quér'e F, Gobert O, Perdrix M, Martin P, Audebert P, Gauthier J C, Geindre J P and Wittmann T 2004 *Phys. Rev. E* **69** 026402
[19] Dromey B, Kar S, Zepf M and Foster P 2004 *Rev. Sci. Instrum.* **75** 645–9
[20] Lévy A *et al* 2007 *Opt. Lett.* **32** 310
[21] Nomura Y, Veisz L, Schmid K, Wittmann T, Wild J and Krausz F 2007 *New J. Phys.* **9** 9
[22] Hörlein R *et al* 2008 *New J. Phys.* **10** 083002
[23] Kim I, Choi I W, Lee S K, Janulewicz K A, Sung J H, Yu T J, Kim H T, Yun H, Jeong T M and Lee J 2011 *Appl. Phys. B* **104** 81–86
[24] Rödel C, Heyer M, Behmke M, Kübel M, Jäckel O, Ziegler W, Ehrt D, Kaluza M C and Paulus G G 2011 *Appl. Phys. B* **103** 295–302
[25] Scott G G *et al* 2015 *New J. Phys.* **17** 033027
[26] Obst L *et al* 2018 *Plasma Phys. Control. Fusion* **60** 054007
[27] Underwood C I D, Gan G, He Z H, Murphy C D, Thomas A G R, Krushelnick K and Nees J 2020 *Laser Part. Beams* **38** 128–34
[28] Choi I W *et al* 2020 *Opt. Lett.* **45** 6342
[29] Kon A *et al* 2022 *High Power Laser Sci. Eng.* **10** e25
[30] Sokollik T, Shiraishi S, Osterhoff J, Evans E, Gonsalves A J, Nakamura K, Tilborg J V, Lin C, Toth C and Leemans W P 2010 Tape-drive based plasma mirror *AIP Conf. Proc.* 1299 233–7
[31] Shaw B H, Steinke S, van Tilborg J and Leemans W P 2016 *Phys. Plasmas* **23** 063118
[32] Xu N 2023 *High Power Laser Sci. Eng.* **11** e23
[33] Brunel F 1987 *Phys. Rev. Lett.* **59** 52–55
[34] Kruer W L and Estabrook K 1985 *Phys. Fluids* **28** 430–2
[35] Leemans W P, Nagler B, Gonsalves A J, Tóth C, Nakamura K, Geddes C G R, Esarey E, Schroeder C B, Hooker S M and Toth C 2006 *Nat. Phys.* **2** 696–9
[36] Arber T D *et al* 2015 *Plasma Phys. Control. Fusion* **57** 113001
[37] Hooker C J *et al* 2008 Commissioning the astra gemini petawatt ti:sapphire laser system *Conf. on Lasers and Electro-Optics/Quantum Electronics and Laser Science Conf. and Photonic Applications Systems Technologies* (Optica Publishing Group) p JThB2
[38] DuPont 2025 *Kapton® Type FN Polyimide Film—General Specifications* DuPont (available at: https://par.uk.com/files/2411%20Kapton%20Type%20FN.pdf) (Accessed 3 November 2025)
[39] Thaury C *et al* 2007 *Nat. Phys.* **3** 424–9
[40] Streeter M J V *et al* 2011 *New J. Phys.* **13** 023041
[41] Chen X L and Sudan R N 1993 *Phys. Rev. Lett.* **70** 2082–5
[42] Monot P, Auguste T, Gibbon P, Jakober F, Mainfray G, Dulieu A, Louis-Jacquet M, Malka G and Miquel J L 1995 *Phys. Rev. Lett.* **74** 2953–6
[43] Thomas A G R *et al* 2007 *Phys. Rev. Lett.* **98** 095004
[44] Pukhov A and ter Vehn J M 2002 *Appl. Phys. B* **74** 355–61
[45] Lu W, Tzoufras M, Joshi C, Tsung F S, Mori W B, Vieira J, Fonseca R A and Silva L O 2007 *Phys. Rev. Accel. Beams* **10** 061301
[46] National Institute of Standards and Technology Atomic Data for Helium (He) (available at: https://physics.nist.gov/)
[47] Põder K *et al* 2024 *Phys. Rev. Lett.* **132** 195001
[48] Wing M 2019 *Phil. Trans. R. Soc. A* **377** 20180185
[49] Schroeder C B, Esarey E, Geddes C G R, Benedetti C and Leemans W P 2010 *Phys. Rev. Accel. Beams* **13** 101301